

Communication

Tuning Co/Ni Ratio in Co–Ni Bimetallic Hybrid for Electrochemical Detection of Glucose

Junyi Zeng¹, Yanting Yang², Xiaoyu Lei¹, Jinan Deng^{1,*}, Ning Hu^{1,*}  and Jun Yang^{1,*} 

¹ Key Laboratory of Biorheological Science and Technology, Ministry of Education and Bioengineering College, Chongqing University, Chongqing 400030, China; zengjunyi@cqu.edu.cn (J.Z.)

² College of Animal Science and Technology, Southwest University, Chongqing 402460, China

* Correspondence: biojdeng@cqu.edu.cn (J.D.); huning@cqu.edu.cn (N.H.); bioyangjun@cqu.edu.cn (J.Y.)

Abstract: Transition metallic binary alloys have attracted enormous attention in regard to the non-enzymatic detection of glucose due to their high electrocatalytic activities induced by the synergistic effect between the individual metallic species. However, the easy aggregation of the bimetallic particles has limited their performance. Herein, a facile metal–organic framework (MOF)-derived strategy is developed to synthesize a hybrid containing binary Co–Ni nanoparticles decorated on an N-doped porous carbon matrix (Co_xNi_y/N-C) for the non-enzymatic detection of glucose. The Co/Ni ratio in the hybrid is investigated to regulate its electrocatalytic behaviors for glucose sensing. A hybrid with the optimal Co/Ni ratio of 1:1 displays two linear detection ranges (0.5 μM to 1 mM and 1 mM to 10 mM) with a detection limit of 0.11 μM for glucose. The feasibility of using this hybrid-modified SPE for glucose detection in real serum samples has also been validated.

Keywords: cobalt–nickel alloy; metal–organic framework-derived hybrid; glucose; biosensors; electrochemical detection



Citation: Zeng, J.; Yang, Y.; Lei, X.; Deng, J.; Hu, N.; Yang, J. Tuning Co/Ni Ratio in Co–Ni Bimetallic Hybrid for Electrochemical Detection of Glucose. *Chemosensors* **2024**, *12*, 38. <https://doi.org/10.3390/chemosensors12030038>

Received: 30 January 2024

Revised: 21 February 2024

Accepted: 26 February 2024

Published: 4 March 2024



Copyright: © 2024 by the authors. Licensee MDPI, Basel, Switzerland. This article is an open access article distributed under the terms and conditions of the Creative Commons Attribution (CC BY) license (<https://creativecommons.org/licenses/by/4.0/>).

1. Introduction

As one of the most popular chronic diseases, diabetes constitutes a great threat to human health. The number of diabetes patients worldwide is expected to reach 642 million by 2040 [1]. Abnormal glucose levels in the body fluids of patients with diabetes usually increase their risk of diabetes complications, such as blindness, heart disease, kidney failure, and foot damage [2]. Therefore, the effective and accurate detection of glucose levels is crucial for patients with diabetes.

The enzyme-based electrochemical method is a widely used method for glucose detection. However, it suffers from complicated enzyme immobilization procedures and the poor stability of the enzyme. To overcome these limitations, non-enzymatic electrochemical methods have attracted much attention in recent years [3]. Transition metals, such as Co, Ni, and their alloys, have been widely investigated as the catalysts for non-enzymatic glucose sensing due to their low cost and excellent catalytic activities [3–9]. Among these materials, Co–Ni bimetallic alloys have received particular attention for glucose detection due to their synergistic effect on the electro-oxidation of glucose, as well as their tunable electronic and geometric structures [2,10–14]. The rich valence states provided by Co–Ni alloys can offer more active sites than their individual species [13]. However, the easy agglomeration of as-synthesized Co–Ni alloys has severely limited their catalytic performance [14]. Therefore, it is highly desirable to develop a method to prepare a Co–Ni alloy with an optimal microstructure to achieve high electrocatalytic efficiency.

In recent years, metal–organic frameworks (MOFs) with tunable microstructures and compositions have been explored as the templates for synthesizing porous carbon-based hybrids with various microstructures using the pyrolysis process [15]. The as-formed porous carbon matrix exhibits an enhanced electrical conductivity, which is beneficial for the charge transfer during the electrocatalytic process [16,17]. At the same time, the presence

of heteroatoms in the carbon substrate induced by the pyrolysis of the organic ligands can retain the dispersed metal nanoparticles on the substrate and prevent their aggregation, offering abundant active sites for mass transport and electrocatalytic activity [18,19]. Recent studies have shown that the proportion of Co and Ni in the Co–Ni alloy plays an important role in determining its sensing performance for glucose [20–26]. The charge migration and electronic properties of the active sites in the alloy can be modulated by tailoring the Co/Ni ratio, thereby influencing its electrocatalytic performance [21].

Herein, we develop a facile method to prepare a bimetallic Co–Ni hybrid for the detection of glucose. The hybrid containing Co–Ni alloy nanoparticles decorated on a porous N-doped carbon matrix (Co_xNi_y/N-C) is synthesized through the one-step pyrolysis of the MOF precursor. The effects of the Co/Ni ratio in the hybrid on the microstructure and electrocatalytic performance toward glucose are investigated. A hybrid with the optimal Co/Ni ratio shows outstanding performance toward the electro-oxidation of glucose due to the synergetic effect between the Co and Ni species and the presence of the N-dopant in the carbon matrix. This hybrid is also successfully used to determine the glucose levels in real serum samples.

2. Materials and Methods

2.1. Materials

Cobalt nitrate hydrate (Co(NO₃)₂·6H₂O, 99%), nickel nitrate hydrate (Ni(NO₃)₂·6H₂O, 99%), zinc nitrate hydrate (Zn(NO₃)₂·6H₂O, 99%), and sodium hydroxide (NaOH, 98%) were purchased from Sinopharm Chemical Reagent (Shanghai, China). Glucose (99.5%) and 2-methylimidazole (98%) were provided by Yuanye Biological Technology (Shanghai, China). Isopropanol was obtained from Cologne Chemicals (Sichuan, China). Nafion solution was purchased from DuPont (Wilmington, DE, USA). Sodium chloride (NaCl), lactose (Lac), fructose (Fru), ascorbic acid (AA), dopamine (DA), adenosine triphosphate (ATP), and uric acid (UA) were bought from Macklin Biochemical (Shanghai, China). All chemicals were used without further purification. Milli-Q water with a resistance of 18.2 MΩ·cm was used for aqueous solution preparation.

2.2. Synthesis of Co_xNi_y/N-C hybrids

The metal salt aqueous solution was prepared by dissolving a total 6.4 mM of Co(NO₃)₂·6H₂O and Ni(NO₃)₂·6H₂O mixture with different molar ratios (3:1, 1:1 and 1:3) in a 16 mL aqueous solution containing 4 mM Zn(NO₃)₂·6H₂O. The 16 mL of the as-prepared metal salt solution was then mixed with 160 mL of 3.45 M 2-methylimidazole aqueous solution under magnetic stirring at room temperature for 6 h to obtain ZnCoNi-MOF solution. Subsequently, the ZnCoNi-MOF solution was centrifuged at a speed of 10 k rpm for 20 min and washed three times with deionized water, followed by a freeze-drying process for 24 h to obtain ZnCoNi-MOF powder. The as-received ZnCoNi-MOF powder was then annealed at 900 °C for 2 h under N₂ gas to achieve the Co_xNi_y/N-C hybrids with different Co/Ni ratios, labeled as Co₃Ni₁/N-C, Co₁Ni₁/N-C, and Co₁Ni₃/N-C, respectively, according to their feeding ratios. For comparison, Co/N-C and Ni/N-C hybrids were synthesized using the same protocol except for the addition of 6.4 mM of Co(NO₃)₂·6H₂O and 6.4 mM Ni(NO₃)₂·6H₂O, respectively, into the Zn(NO₃)₂·6H₂O aqueous solution to prepare the metal salt solution instead of the Co(NO₃)₂·6H₂O and Ni(NO₃)₂·6H₂O mixture.

2.3. Preparation of Hybrid-Modified Electrodes

Three-electrode system-based screen-printed electrodes (SPEs, Yituo Biosensing Technology, Suzhou, China) were employed as the substrate to investigate the sensing performance of the hybrids for glucose. In bare SPEs, the carbon electrode, Ag/AgCl electrode and carbon electrode were used as the working electrode, reference electrode and counter electrode, respectively. The hybrid ink solution was prepared by dissolving 2 mg hybrid powder into 1 mL isopropanol solution containing 0.5 wt% Nafion. For the modification of the carbon-based working electrode, 5 μL of the hybrid ink was dropped on the working

electrode with an area of 3 mm² and dried at room temperature for 2 h to achieve the hybrid-modified SPE.

2.4. Characterizations

The morphology and elemental composition of the hybrids were characterized using a field emission scanning electron microscope (SEM, Quattro, 20 kV) and a transmission electron microscope (TEM, JEM-2100F, 200 kV), respectively. X-ray diffraction (XRD, Rigaku D/Max 2500, Tokyo, Japan) was used to determine the crystal structure of the samples using Cu K α radiation at 40 kV. The N₂ adsorption–desorption isotherms were measured using a Quadrasorb analyzer at 77 K after the pretreatment of the sample in a vacuum at 473 K for 2 h. The specific surface areas of the hybrids were calculated using the Brunauer–Emmett–Teller (BET) method.

2.5. Electrochemical Measurements

Cyclic voltammetry (CV) and amperometry measurements (i-t) were employed to evaluate the electrochemical performance of the hybrid-modified SPEs, which were performed in an electrochemical cell containing 100 mL 0.1 M NaOH aqueous solution using CHI660E electrochemical workstation from Shanghai Chenhua Instrument Co., Ltd. (Shanghai, China). For the i-t measurement, different concentrations of glucose were successively added into a 0.1 M NaOH aqueous solution every 50 s at the applied potential of 0.6 V.

3. Results

3.1. Morphology and Structure Characterization

The hybrids were obtained through the pyrolysis of MOF precursors at 900 °C for 2 h under N₂ gas. During the calcination process, the Zn species were evaporated and the organic linkers containing a rich nitrogen source were carbonized, forming an N-doped porous carbon substrate decorated with metallic particles [27]. The Co/N-C and Ni/N-C hybrids were synthesized for comparison. The morphologies of the as-prepared hybrids were characterized by SEM. As shown in Figure 1a,b, the Co/N-C and Ni/N-C hybrids exhibit a porous structure decorated with particles of irregular morphologies and tubular structures. For Co₃Ni₁/N-C and Co₁Ni₁/N-C hybrids, uniformly distributed spherical particles are formed on the substrate (Figure 1c,d). However, after a further increase in the Ni content to a Co/Ni ratio of 1:3, the particles show irregular spherical shapes and aggregation (Figure 1e). We further calculated the specific surface areas of the hybrids using the BET method (Figure S1 and Table S1). Among these hybrids, the Co₁Ni₁/N-C hybrid displays the highest specific surface area of 375.64 m²/g, beneficial for mass transport [21]. The TEM and the corresponding EDS elemental mapping images confirm the homogenous distribution of C, N, O, Co, and Ni elements in the Co_xNi_y/N-C hybrids (Figures 1f and S2). The uniform distributions of Ni and Co on the carbon matrix at the same location in the hybrids support the formation of the Co–Ni binary alloy on the carbon matrix.

The crystalline structures of the as-prepared hybrids were analyzed using XRD. The XRD patterns of Co_xNi_y/N-C hybrids are similar to those of the Co/N-C and Ni/N-C hybrids (Figure 2a). The relative broad peak at 26° was assigned to the (002) plane of graphitic carbon (JCPDS No. 89-8487) [20]. There are three diffraction peaks at around 44°, 52°, and 76°, which are indexed to the (111), (200), and (220) planes of the face-centered cubic (FCC) structures of Co (JCPDS No. 04-0850) and Ni (JCPDS No. 04-0850), respectively [28]. No other obvious peaks are observed, suggesting the evaporation of the Zn species during the pyrolysis process. Figure 2b shows the zoomed-in (111) peak of the hybrids. Compared with pristine Co/N-C, the zoomed-in (111) peak of the Co_xNi_y/N-C hybrid gradually shifts towards a higher 2 θ value with the increase in the Ni amount. This is due to the lattice contraction of the Ni alloying with Co, confirming the formation of the Co–Ni alloy [20,29]. No other planes were observed for the Co_xNi_y/N-C hybrids, implying that the formation of the Co–Ni alloy has not destroyed the crystal structure of Co or Ni due to the similar lattice parameters of Co and Ni.

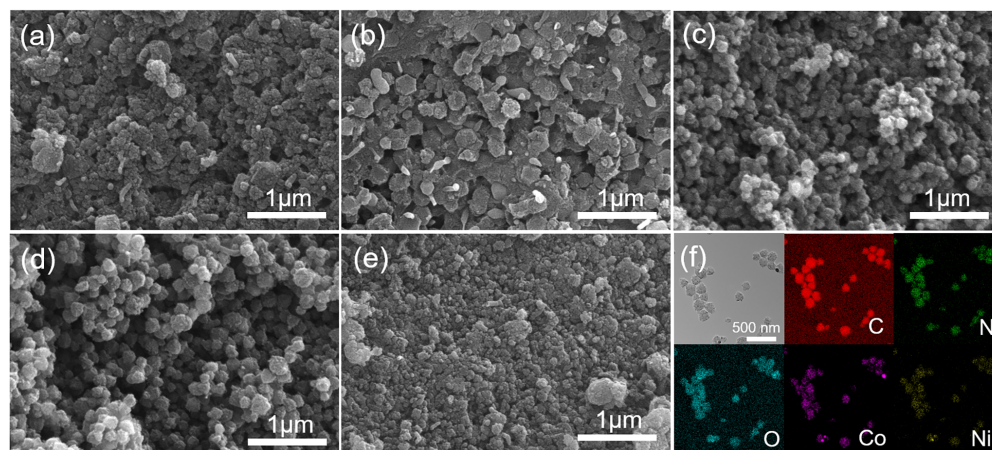


Figure 1. SEM images of (a) Co/N-C, (b) Ni/N-C, (c) $\text{Co}_3\text{Ni}_1/\text{N-C}$, (d) $\text{Co}_1\text{Ni}_1/\text{N-C}$, and (e) $\text{Co}_1\text{Ni}_3/\text{N-C}$ hybrids. (f) TEM and EDS mapping images of the $\text{Co}_1\text{Ni}_1/\text{N-C}$ hybrid for C, N, O, Co, and Ni.

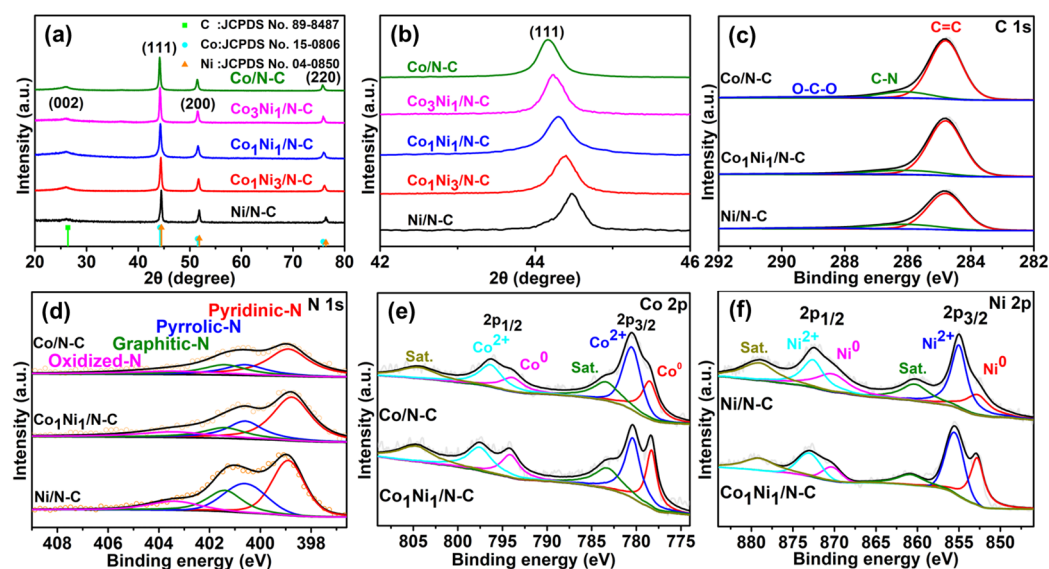


Figure 2. XRD patterns (a) and the corresponding zoomed-in XRD patterns (b) of the hybrids. XPS spectra of C 1s (c), N 1s (d), Co 2p (e), and Ni 2p (f) for the Co/N-C, Ni/N-C, and $\text{Co}_1\text{Ni}_1/\text{N-C}$ hybrids.

The chemical compositions and valence states of the elements in the hybrids were characterized using XPS (Figures 2c–f and S3). Three peaks in the high-resolution C 1s spectra located at 284.8 eV, 285.6 eV, and 289.1 eV, are assigned to C=C, C-N and O-C-O, respectively (Figure 2c) [30]. The existence of C=C and C-N indicates the graphite carbon structure and the doping of N in the carbon matrix during the pyrolysis of the MOF precursors, respectively [30]. For the N 1s spectra, four peaks at 398.9 eV, 400.6 eV, 401.4 eV, and 403.4 eV are ascribed to pyridinic-N, pyrrolic-N, graphitic-N, and oxidized-N, respectively (Figure 2d) [31]. It has been reported that the presence of pyridinic-N and pyrrolic-N can provide active sites and increase the charge density for electrocatalytic reactions by tailoring the electronic properties of the carbon substrate with their lone pair of electrons [32–34]. The amount of pyridinic-N and pyrrolic-N in the $\text{Co}_1\text{Ni}_1/\text{N-C}$ hybrid (72.1%) is the highest among these hybrids (68.3% for Co/N-C, 69.5% for Ni/N-C, 71.4% for $\text{Co}_3\text{Ni}_1/\text{N-C}$, and 70.1% for $\text{Co}_1\text{Ni}_3/\text{N-C}$, respectively) (Table S2). Meanwhile, it has been shown that the existence of the N dopant can prevent the aggregation of the metallic particles [19]. Figures 2e and S3 reveal that the Co 2p spectra of the $\text{Co}_x\text{Ni}_y/\text{N-C}$ and Co/N-C hybrids compose the two main peaks of Co 2p_{3/2} and Co 2p_{1/2}, which are further

deconvoluted into four subpeaks, corresponding to Co⁰ (~778.5 eV and ~794.1 eV) and Co²⁺ (~780.4 eV and ~797.0 eV), and two satellites at around 784.4 eV and 804.2 eV [15]. The Ni 2p spectra of the Co_xNi_y/N-C and Ni/N-C hybrids have confirmed the presence of metallic Ni at around 852.8 eV and 870.3 eV, respectively (Figures 2f and S3) [35,36]. The peaks attributed to Ni 2p_{3/2} (~855.0 eV), Ni 2p_{1/2} (~872.6 eV) and two satellites (~860.3 eV and ~879.1 eV, respectively) are Ni²⁺ [15]. The presence of Co⁰ and Ni⁰ confirms the reduction of Co²⁺ and Ni²⁺ species during the pyrolysis, while the existence of Co²⁺ and Ni²⁺ in the hybrids indicates the surface oxidation by the atmosphere [29,37].

3.2. Electrochemical Performance of the Hybrid

The electrochemical activities of the Co_xNi_y/N-C hybrids were evaluated in an electrochemical cell containing 100 mL 0.1 M NaOH aqueous solution using Co_xNi_y/N-C hybrid-modified SPEs. For comparison, bare SPE, Co/N-C hybrid-modified SPE, and Ni/N-C hybrid-modified SPE were also measured under the same conditions. Figure 3a shows the CV curves of the SPEs with and without the modification of the hybrids in a 0.1 M NaOH aqueous solution at a scan rate of 50 mV·s⁻¹. The current of the hybrid-modified SPEs shows a huge improvement compared with that of the bare SPE. The Ni/N-C-modified SPE shows an anodic peak current at around 0.51 V, indicating the oxidation of Ni²⁺ to Ni³⁺, while the Co/N-C-modified SPE exhibits an anodic peak current of Co²⁺ to Co³⁺ at around 0.16 V [21]. Although the oxidation peaks of the Co₃Ni₁/N-C and Co₁Ni₃/N-C are located between those of the pristine Co/N-C and Ni/N-C hybrids due to the formation of the Co–Ni alloy, the peak current is smaller than that of the pristine Ni/N-C (Figure 3a). Interestingly, the Co₁Ni₁/N-C displays the highest oxidation current among the hybrids, indicating the significant role of the Co/Ni ratio in dictating the electrocatalytic performance of the hybrid.

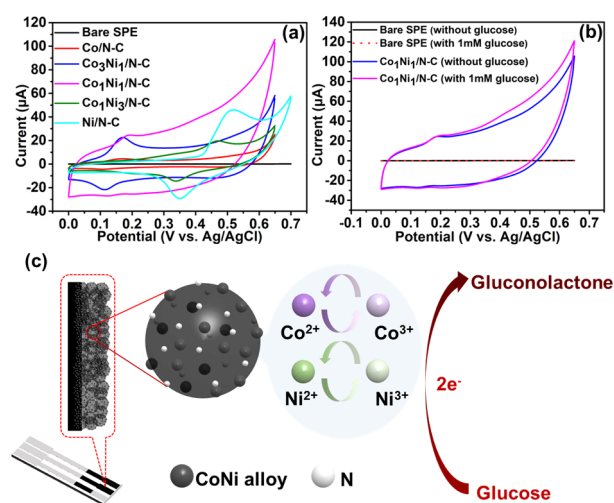
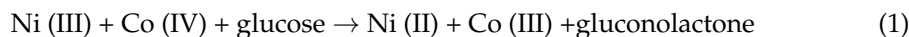


Figure 3. (a) CV curves of SPEs with and without the modification of the hybrid in 0.1 M NaOH aqueous solution at a scan rate of 50 mV·s⁻¹. (b) CV curves of the bare SPE and Co₁Ni₁/N-C hybrid-modified SPE in 0.1 M NaOH aqueous solution in the absence and presence of 1 mM glucose at a scan rate of 50 mV·s⁻¹. (c) Schematic illustration of the electro-oxidation of glucose on the Co–Ni hybrid-modified SPE.

We further investigated the performance of hybrid-modified SPEs in the presence of 1 mM glucose. As shown in Figure 3b, after the addition of 1 mM glucose, the oxidation current of the Co₁Ni₁/N-C hybrid-modified SPE shows an increase starting from around 0.2 V, while the current of the bare SPE hardly changes, indicating high electrocatalytic activity toward the glucose of the hybrid. An obvious increase in the oxidation current was also observed for other types of hybrid-modified SPEs in the presence of 1 mM glucose (Figure S4). Additionally, the Co_xNi_y/N-C hybrid starts to show the current increment

at around 0.2 V, which is lower than that of the pristine Co/N-C (~0.4 V) and Ni/N-C (~0.5 V) hybrids (Figure S4). The lower onset oxidation potential of the Co_xNi_y/N-C hybrid indicates the synergistic effect between the Co and Ni species for the easier electro-oxidation of glucose. The sensing mechanism can be explained as follows [15],



In the alkaline solution, high-valence metallic species, Ni (III) and Co (IV), are responsible for the oxidation of glucose to gluconolactone (Figure 3c). Meanwhile, the synergistic effect between the Co and Ni species, along with the porous N-doped carbon network, provides large active sites and promotes the electron transfer process, thereby promoting the electro-oxidation of glucose.

We also found that the hybrid-modified SPEs showed the largest current increment at around 0.6 V in the presence of 1 mM glucose. At the oxidation potential of 0.6 V, the Co₁Ni₁/N-C hybrid-modified SPE exhibits the largest current increment, further confirming the optimal Co/Ni ratio of 1:1 for glucose sensing (Figure S5). Therefore, the Co₁Ni₁/N-C hybrid-modified SPE was employed as the optimal electrode for the subsequent studies of glucose detection.

3.3. Glucose Detection with the Co₁Ni₁/N-C Hybrid-Modified SPE

Figure 4a shows the CV curves of the Co₁Ni₁/N-C hybrid-modified SPEs in the presence of 1 mM glucose at different scan rates ranging from 2.5 mV/s to 150 mV/s. Both anodic and cathodic currents increase with the increase in the scan rate in the presence of 1 mM glucose. The anodic current at 0.6 V linearly increases with the square root of the scan rate, suggesting that the glucose oxidation is a diffusion-controlled process (inset in Figure 4a) [38]. Figure 4b indicates that the oxidation current of the Co₁Ni₁/N-C hybrid-modified SPE increases with the increase in the glucose concentration from 0 mM to 10 mM. We further plotted the oxidation current of the Co₁Ni₁/N-C hybrid-modified SPE as a function of glucose concentration at different applied potentials (Figure S6a). The sensitivity of the Co₁Ni₁/N-C hybrid-modified SPE for glucose oxidation reaches the maximum at the applied potential of 0.6 V (Figure S6b). Therefore, the applied potential of 0.6 V was employed to perform i-t measurement of the Co₁Ni₁/N-C hybrid-modified SPE for glucose in a 0.1 M NaOH aqueous solution.

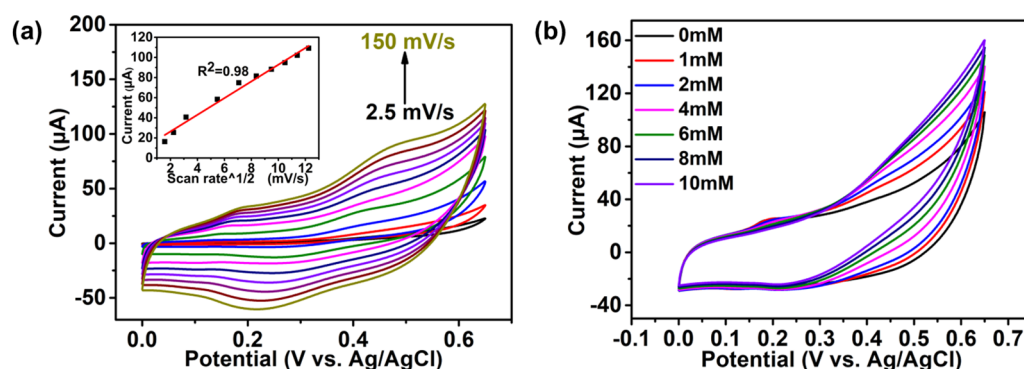


Figure 4. CV curves of the Co₁Ni₁/N-C hybrid-modified SPE in aqueous solutions containing (a) 1 mM glucose at various scan rates (inset: the corresponding anodic peak current as a function of the square root of the scan rate at the applied potential of 0.6 V), and (b) different concentrations of glucose at a scan rate of 50 mV·s⁻¹.

The amperometric response of Co₁Ni₁/N-C hybrid-modified SPEs was recorded by successive addition of various concentrations of glucose into a 0.1 M NaOH aqueous solution under magnetic stirring conditions (Figure 5a). A steady current can be achieved in less than 5 s after each addition of glucose. We find that the response current at 50 s of the Co₁Ni₁/N-C hybrid-modified SPEs to glucose shows two linear ranges (Figure 5b). The low

linear range is from 0.5 μM to 1 mM ($R^2 = 0.987$) with a sensitivity of $1041.7 \mu\text{A} \cdot \text{mM}^{-1} \cdot \text{cm}^{-2}$ (inset in Figure 5b). The linear range in the high concentration region is from 1 mM to 10 mM ($R^2 = 0.980$) with a sensitivity of $75.7 \mu\text{A} \cdot \text{mM}^{-1} \cdot \text{cm}^{-2}$. The detection limit was estimated to be 0.11 μM ($S/N = 3$), which is lower than most similar non-enzymatic glucose sensors reported (Table S3).

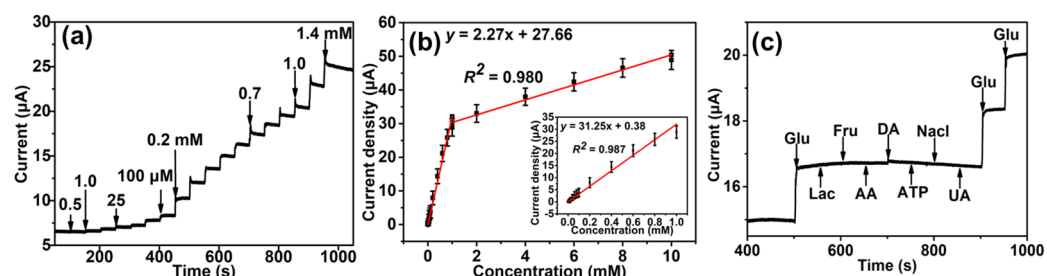


Figure 5. Amperometric response of the $\text{Co}_1\text{Ni}_1/\text{N-C}$ hybrid-modified SPE after successive addition of different concentrations of glucose into a 0.1 M NaOH aqueous solution (a) and the corresponding calibration curve for glucose detection (inset: linear fitting of the low concentration regime) (b). (c) Amperometric response of the $\text{Co}_1\text{Ni}_1/\text{N-C}$ hybrid-modified SPE after the successive addition of glucose and interferences.

Lac, Fru, AA, UA, DA, ATP, and NaCl, which coexist with glucose in biological fluids, are major interference species for the detection of glucose. We studied the current response of the $\text{Co}_1\text{Ni}_1/\text{N-C}$ hybrid-modified SPE after the successive addition of 1 mM glucose and interferences of 2 mM Lac, 2 mM Fru, 2 mM AA, 2 mM UA, 2 mM DA, 2 mM ATP, and 30 mM NaCl in the 0.1 M NaOH aqueous solution (Figure 5c). However, we found that compared with the current change induced by 1 mM glucose, the $\text{Co}_1\text{Ni}_1/\text{N-C}$ hybrid-modified SPE exhibits a negligible current change after the addition of interferences, indicating the good selectivity of the $\text{Co}_1\text{Ni}_1/\text{N-C}$ hybrid-modified SPE.

The reproducibility of the $\text{Co}_1\text{Ni}_1/\text{N-C}$ hybrid-modified SPE was evaluated using five independent electrodes for the detection of 1 mM glucose in a 0.1 M NaOH aqueous solution (Figure 6a). The relative standard deviation (RSD) of the five current responses is 4.84%, indicating the good reproducibility of the electrode. The stability experiment was conducted by measuring the current response of the prepared $\text{Co}_1\text{Ni}_1/\text{N-C}$ hybrid-modified SPE for 1 mM glucose for 7 days. As shown in Figure 6b, the $\text{Co}_1\text{Ni}_1/\text{N-C}$ hybrid-modified SPE retained 90.22% of the initial responses for 1 mM glucose after 7 days, suggesting good stability.

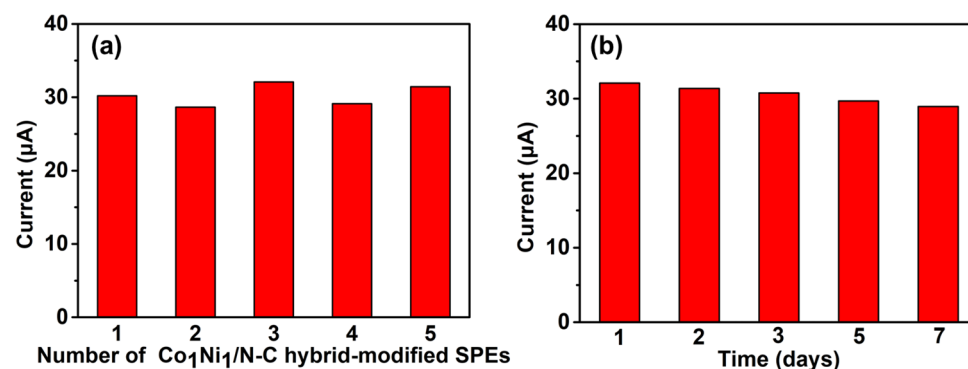


Figure 6. The current response of the $\text{Co}_1\text{Ni}_1/\text{N-C}$ hybrid-modified SPE (a) was evaluated using five independent electrodes and (b) was evaluated at different days for the detection of 1 mM glucose in a 0.1 M NaOH aqueous solution.

3.4. Glucose Detection Using Real Samples

To assess the feasibility of the Co₁Ni₁/N-C hybrid-modified SPE, human serum samples were collected from volunteers in Chongqing University Hospital to evaluate the glucose sensing performance. The samples were used for the experiment with the consent of the volunteers and Chongqing University Hospital. For analysis, 6 μ L serum was first diluted using 24 μ L 0.1 M NaOH aqueous solution and then dropped on the SPE. Amperometry measurement (i-t) was performed at the applied potential of 0.6 V for 60 s to determine the glucose concentration in the diluted serum samples (Figure S7). The current response at 50 s was extracted to calculate the corresponding glucose concentration based on the calibration curve. For comparison, a blood glucose meter and its electrode (accuracy: $\leq \pm 20\%$, precision: CV < 7.5%, Yuwell 660, Zhenjiang, China) were employed to determine the glucose levels in the serum samples. As shown in Table 1, compared with the glucose concentration determined by the glucose meter, the Co₁Ni₁/N-C hybrid-modified SPE shows similar results with a relative standard deviation (RSD) of less than 3.01%. These results indicate that the Co₁Ni₁/N-C hybrid-modified SPE demonstrates good feasibility for detecting glucose in real samples.

Table 1. Glucose detection in human serum samples using a blood glucose meter and the Co₁Ni₁/N-C hybrid-modified SPE.

Samples	Blood Glucose Meter (mM)	Co ₁ Ni ₁ /N-C Hybrid-Modified SPE (mM)	RSD (%)
1	6.6	6.61 \pm 0.12	1.82
2	4.0	4.02 \pm 0.09	2.24
3	5.4	5.32 \pm 0.16	3.01
4	4.6	4.58 \pm 0.11	2.40

4. Conclusions

In summary, Co_xNi_y/N-C hybrids with different Co/Ni ratios were synthesized through the carbonization of MOF precursors. The obtained hybrids exhibited good electrocatalytic activities toward glucose. We found that the microstructure and electrocatalytic performance of the hybrid are dependent on the Co/Ni ratio. The hybrid-modified SPE with the optimal Co/Ni ratio of 1:1 for the electro-oxidation of glucose shows two linear detection ranges (0.5 μ M to 1 mM, 1 mM to 10 mM) with a sensitivity of 1041.7 μ A \cdot mM⁻¹ \cdot cm⁻² and 75.7 μ A \cdot mM⁻¹ \cdot cm⁻², respectively. The detection limit of the Co₁Ni₁/N-C hybrid-modified SPE for glucose was calculated as being as low as 0.11 μ M. The high-sensing performance of the Co₁Ni₁/N-C hybrid can be ascribed to the synergistic effect between the Co and Ni species, along with the porous N-dopant carbon matrix. The feasibility of the Co₁Ni₁/N-C hybrid-modified SPE for glucose detection in real serum samples was also validated, indicating a promising candidate for the non-enzymatic detection of glucose.

Supplementary Materials: The supporting information can be downloaded at: <https://www.mdpi.com/article/10.3390/chemosensors12030038/s1>. Figure S1: N₂ adsorption/desorption isotherm of Co₁Ni₁/N-C hybrid; Table S1: Specific surface areas of hybrids calculated by BET method; Figure S2: The TEM images and the corresponding elemental mapping images of (a) Co₃Ni₁/N-C and (b) Co₁Ni₃/N-C hybrids for C, N, O, Co, and Ni. The scale bar is 500 nm; Figure S3: XPS spectra of C 1s, N 1s, Co 2p, and Ni 2p for (a) Co₃Ni₁/N-C and (b) Co₁Ni₃/N-C hybrids; Table S2: N contents calculated from XPS spectra; Figure S4: CV curves of SPEs modified with (a) Co/N-C, (b) Ni/N-C, (c) Co₁Ni₃/N-C, and (d) Co₃Ni₁/N-C hybrids in 0.1 M NaOH aqueous solution in the absence and presence of 1 mM glucose at a scan rate of 50 mV \cdot s⁻¹; Figure S5: The current increment extracted from the CVs of hybrid-modified SPEs with different Co/Ni ratios at 0.6 V in presence of 1 mM glucose at a scan rate of 50 mV \cdot s⁻¹; Figure S6: Current response of Co₁Ni₁/N-C-modified SPE as a function of glucose concentration in 0.1 NaOH aqueous solution at various applied potentials (a) and the corresponding sensitivity at different applied potentials (b); Table S3: Comparison of the sensing performance of Co₁Ni₁/N-C hybrid-modified SPE prepared in this work with other non-enzymatic

glucose sensors; Figure S7: Amperometric response of CO₁Ni₁/N-C hybrid-modified SPE for glucose determination using serum samples.

Author Contributions: Conceptualization, J.D. and J.Y.; methodology, J.Z.; validation, J.Z., Y.Y. and X.L.; formal analysis, J.Z.; investigation, Y.Y.; writing—original draft preparation, J.Z.; writing—review and editing, J.D., N.H. and J.Y.; visualization, N.H.; supervision, N.H. and J.Y. All authors have read and agreed to the published version of the manuscript.

Funding: This research was funded by the National Natural Science Foundation of China (Nos. 32101114 and 21827812), China Postdoctoral Science Foundation (No. 2021M700603).

Data Availability Statement: Data will be made available on request.

Conflicts of Interest: The authors declare no conflicts of interest.

References

1. Teymourian, H.; Barfidokht, A.; Wang, J. Electrochemical glucose sensors in diabetes management: An updated review (2010–2020). *Chem. Soc. Rev.* **2020**, *49*, 7671–7709. [[CrossRef](#)] [[PubMed](#)]
2. Sehit, E.; Altintas, Z. Significance of nanomaterials in electrochemical glucose sensors: An updated review (2016–2020). *Biosens. Bioelectron.* **2020**, *159*, 112165. [[CrossRef](#)]
3. Wei, M.; Qiao, Y.; Zhao, H.; Liang, J.; Li, T.; Luo, Y.; Lu, S.; Shi, X.; Lu, W.; Sun, X. Electrochemical non-enzymatic glucose sensors: Recent progress and perspectives. *Chem. Commun.* **2020**, *56*, 14553–14569. [[CrossRef](#)] [[PubMed](#)]
4. Emir, G.; Dilgin, Y.; Ramanaviciene, A.; Ramanavicius, A. Amperometric nonenzymatic glucose biosensor based on graphite rod electrode modified by Ni-nanoparticle/polypyrrole composite. *Microchem. J.* **2021**, *161*, 105751. [[CrossRef](#)]
5. Marini, S.; Ben Mansour, N.; Hjiri, M.; Dhahri, R.; El Mir, L.; Espro, C.; Bonavita, A.; Galvagno, S.; Neri, G.; Leonardi, S.G. Non-enzymatic glucose sensor based on nickel/carbon composite. *Electroanalysis* **2018**, *30*, 727–733. [[CrossRef](#)]
6. Ayaz, S.; Karakaya, S.; Emir, G.; Dilgin, D.G.; Dilgin, Y. A novel enzyme-free fi-amperometric glucose biosensor at cu nanoparticles modified graphite pencil electrode. *Microchem. J.* **2020**, *154*, 104586. [[CrossRef](#)]
7. Xu, J.; Li, F.; Wang, D.; Nawaz, M.H.; An, Q.; Han, D.; Niu, L. Co₃O₄ nanostructures on flexible carbon cloth for crystal plane effect of nonenzymatic electrocatalysis for glucose. *Biosens. Bioelectron.* **2019**, *123*, 25–29. [[CrossRef](#)]
8. Nacef, M.; Chelaghmia, M.L.; Affoune, A.M.; Pontié, M. Electrochemical investigation of glucose on a highly sensitive nickel-copper modified pencil graphite electrode. *Electroanalysis* **2019**, *31*, 113–120. [[CrossRef](#)]
9. Wang, L.; Lu, X.; Ye, Y.; Sun, L.; Song, Y. Nickel-cobalt nanostructures coated reduced graphene oxide nanocomposite electrode for nonenzymatic glucose biosensing. *Electrochim. Acta* **2013**, *114*, 484–493. [[CrossRef](#)]
10. Huang, W.; Cao, Y.; Chen, Y.; Peng, J.; Lai, X.; Tu, J. Fast synthesis of porous NiCo₂O₄ hollow nanospheres for a high-sensitivity non-enzymatic glucose sensor. *Appl. Surf. Sci.* **2017**, *396*, 804–811. [[CrossRef](#)]
11. Yang, J.; Cho, M.; Lee, Y. Synthesis of hierarchical NiCo₂O₄ hollow nanorods via sacrificial-template accelerate hydrolysis for electrochemical glucose oxidation. *Biosens. Bioelectron.* **2016**, *75*, 15–22. [[CrossRef](#)] [[PubMed](#)]
12. Hwang, D.W.; Lee, S.; Seo, M.; Chung, T.D. Recent advances in electrochemical non-enzymatic glucose sensors—A review. *Anal. Chim. Acta* **2018**, *1033*, 1–34. [[CrossRef](#)] [[PubMed](#)]
13. Rao, H.; Zhang, Z.; Ge, H.; Liu, X.; Zou, P.; Wang, X.; Wang, Y. Enhanced amperometric sensing using a NiCo₂O₄/nitrogen-doped reduced graphene oxide/ionic liquid ternary composite for enzyme-free detection of glucose. *New J. Chem.* **2017**, *41*, 3667–3676. [[CrossRef](#)]
14. Zheng, W.; Li, Y.; Lee, L.Y.S. Insights into the transition metal ion-mediated electrooxidation of glucose in alkaline electrolyte. *Electrochim. Acta* **2019**, *308*, 9–19. [[CrossRef](#)]
15. Wang, L.; Hou, C.; Yu, H.; Zhang, Q.; Li, Y.; Wang, H. Metal-organic framework-derived nickel/cobalt-based nanohybrids for sensing non-enzymatic glucose. *ChemElectroChem* **2020**, *7*, 4446–4452. [[CrossRef](#)]
16. Adeel, M.; Asif, K.; Rahman, M.M.; Daniele, S.; Canzonieri, V.; Rizzolio, F. Glucose detection devices and methods based on metal-organic frameworks and related materials. *Adv. Funct. Mater.* **2021**, *31*, 2106023. [[CrossRef](#)]
17. Xie, Y.; Feng, C.; Guo, Y.; Li, S.; Guo, C.; Zhang, Y.; Wang, J. Mofs derived carbon nanotubes coated coni alloy nanocomposites with n-doped rich-defect and abundant cavity structure as efficient trifunctional electrocatalyst. *Appl. Surf. Sci.* **2021**, *536*, 147786. [[CrossRef](#)]
18. Shen, Y.; Pan, T.; Wang, L.; Ren, Z.; Zhang, W.; Huo, F. Programmable logic in metal-organic frameworks for catalysis. *Adv. Mater.* **2021**, *33*, 2007442. [[CrossRef](#)]
19. Niu, X.; Bo, X.; Guo, L. Ultrasensitive simultaneous voltammetric determination of 4-aminophenol and acetaminophen based on bimetallic mof-derived nitrogen-doped carbon coated coni alloy. *Anal. Chim. Acta* **2021**, *1145*, 37–45. [[CrossRef](#)]
20. Ning, H.; Li, G.; Chen, Y.; Zhang, K.; Gong, Z.; Nie, R.; Hu, W.; Xia, Q. Porous N-doped carbon-encapsulated CoNi alloy nanoparticles derived from MOFs as efficient bifunctional oxygen electrocatalysts. *ACS Appl. Mater. Interfaces* **2019**, *11*, 1957–1968. [[CrossRef](#)]

21. Zou, H.; Tian, D.; Lv, C.; Wu, S.; Lu, G.; Guo, Y.; Liu, Y.; Yu, Y.; Ding, K. The synergistic effect of Co/Ni in ultrathin metal-organic framework nanosheets for the prominent optimization of non-enzymatic electrochemical glucose detection. *J. Mater. Chem. B* **2020**, *8*, 1008–1016. [[CrossRef](#)] [[PubMed](#)]
22. Xu, Z.; Wang, Q.; Zhangsun, H.; Zhao, S.; Zhao, Y.; Wang, L. Carbon cloth-supported nanorod-like conductive Ni/Co bimetal MOF: A stable and high-performance enzyme-free electrochemical sensor for determination of glucose in serum and beverage. *Food Chem.* **2021**, *349*, 129202. [[CrossRef](#)]
23. Wu, Y.T.; Tsao, P.K.; Chen, K.J.; Lin, Y.C.; Aulia, S.; Chang, L.Y.; Ho, K.C.; Chang, C.Y.; Mizuguchi, H.; Yeh, M.H. Designing bimetallic ni-based layered double hydroxides for enzyme-free electrochemical lactate biosensors. *Sens. Actuators B Chem.* **2021**, *346*, 130505. [[CrossRef](#)]
24. Shu, Y.; Su, T.; Lu, Q.; Shang, Z.; Xu, Q.; Hu, X. Highly stretchable wearable electrochemical sensor based on Ni-Co MOF nanosheet-decorated Ag/rGO/PU fiber for continuous sweat glucose detection. *Anal. Chem.* **2021**, *93*, 16222–16230. [[CrossRef](#)] [[PubMed](#)]
25. Amin, K.M.; Muench, F.; Kunz, U.; Ensinger, W. 3D NiCo-Layered double Hydroxide@ Ni nanotube networks as integrated free-standing electrodes for nonenzymatic glucose sensing. *J. Colloid Interface Sci.* **2021**, *591*, 384–395. [[CrossRef](#)] [[PubMed](#)]
26. Li, W.; Lv, S.; Wang, Y.; Zhang, L.; Cui, X. Nanoporous gold induced vertically standing 2D NiCo bimetal-organic framework nanosheets for non-enzymatic glucose biosensing. *Sens. Actuators B Chem.* **2019**, *281*, 652–658. [[CrossRef](#)]
27. Li, J.; Wang, Y.; Yin, Z.; He, R.; Wang, Y.; Qiao, J. In-situ growth of CoNi bimetal anchored on carbon nanoparticle/nanotube hybrid for boosting rechargeable Zn-air battery. *J. Energy Chem.* **2022**, *66*, 348–355. [[CrossRef](#)]
28. Sheng, Q.; Liu, D.; Zheng, J. NiCo alloy nanoparticles anchored on polypyrrole/reduced graphene oxide nanocomposites for nonenzymatic glucose sensing. *New J. Chem.* **2016**, *40*, 6658–6665. [[CrossRef](#)]
29. Gao, Z.; Wang, L.; Chang, J.; Chen, C.; Wu, D.; Xu, F.; Jiang, K. CoNi alloy incorporated, N doped porous carbon as efficient counter electrode for dye-sensitized solar cell. *J. Power Sources* **2017**, *348*, 158–167. [[CrossRef](#)]
30. Chen, L.; Xu, Z.; Han, W.; Zhang, Q.; Bai, Z.; Chen, Z.; Li, G.; Wang, X. Bimetallic conical alloy nanoparticles embedded in pomegranate-like nitrogen-doped carbon spheres for electrocatalytic oxygen reduction and evolution. *ACS Appl. Nano Mater.* **2020**, *3*, 1354–1362. [[CrossRef](#)]
31. Dilpazir, S.; Liu, R.; Yuan, M.; Imran, M.; Liu, Z.; Xie, Y.; Zhao, H.; Zhang, G. Br/Co/N co-doped porous carbon frameworks with enriched defects for high-performance electrocatalysis. *J. Mater. Chem. A* **2020**, *8*, 10865–10874. [[CrossRef](#)]
32. Mo, G.; Zheng, X.; Ye, N.; Ruan, Z. Nitrogen-doped carbon dodecahedron embedded with cobalt nanoparticles for the direct electro-oxidation of glucose and efficient nonenzymatic glucose sensing. *Talanta* **2021**, *225*, 121954. [[CrossRef](#)] [[PubMed](#)]
33. Emran, M.Y.; Shenashen, M.A.; Elmarakbi, A.; Selim, M.M.; El-Safty, S.A. Nitrogen-doped carbon hollow trunk-like structure as a portable electrochemical sensor for noradrenaline detection in neuronal cells. *Anal. Chim. Acta* **2022**, *1192*, 339380. [[CrossRef](#)]
34. Wang, H.; Maiyalagan, T.; Wang, X. Review on recent progress in nitrogen-doped graphene: Synthesis, characterization, and its potential applications. *ACS Catal.* **2012**, *2*, 781–794. [[CrossRef](#)]
35. Lee, S.; Kang, J.-S.; Leung, K.T.; Kim, S.K.; Sohn, Y. Magnetic Ni-Co alloys induced by water gas shift reaction, Ni-Co oxides by co oxidation and their supercapacitor applications. *Appl. Surf. Sci.* **2016**, *386*, 393–404. [[CrossRef](#)]
36. Wang, J.; Liu, Y.; Cheng, L.; Chen, R.; Ni, H. Quasi-aligned nanorod arrays composed of nickel–cobalt nanoparticles anchored on TiO₂/C nanofiber arrays as free standing electrode for enzymeless glucose sensors. *J. Alloys Compd.* **2020**, *821*, 153510. [[CrossRef](#)]
37. Chen, M.J.; Zhang, D.X.; Li, D.; Ke, S.-C.; Ma, X.-C.; Chang, G.-G.; Chen, J.; Yang, X.-Y. All-around coating of CoNi nanoalloy using a hierarchically porous carbon derived from bimetallic MOFs for highly efficient hydrolytic dehydrogenation of ammonia-borane. *New J. Chem.* **2020**, *44*, 3021–3027. [[CrossRef](#)]
38. Wang, L.; Yu, H.; Zhang, Q.; Li, Y.; Jia, W.; Hou, C.; Wang, H. NiCo–NiCoO₂/carbon hollow nanocages for non-enzyme glucose detection. *Electrochim. Acta* **2021**, *381*, 138259. [[CrossRef](#)]

Disclaimer/Publisher’s Note: The statements, opinions and data contained in all publications are solely those of the individual author(s) and contributor(s) and not of MDPI and/or the editor(s). MDPI and/or the editor(s) disclaim responsibility for any injury to people or property resulting from any ideas, methods, instructions or products referred to in the content.